Öner, B., Pomeroy, J. W., & Kuball, M. (2020). Time Resolved Hyperspectral Quantum Rod Thermography of Microelectronic Devices: Temperature Transients in a GaN HEMT. *IEEE Electron Device Letters*. https://doi.org/10.1109/LED.2020.2989919

Time Resolved Hyperspectral Quantum Rod Thermography of Microelectronic Devices: Temperature Transients in a GaN HEMT

Bahar Öner, James W. Pomeroy, and Martin Kuball, *Fellow, IEEE*

***Abstract*— The trend of miniaturization and rapid progress in the cost-competitive microelectronic industry require high resolution, fast, accurate and cost-effective thermal characterization techniques. These techniques aid the assessment of reliability and performance benchmarking of new device designs for the realistic operation conditions. We present a time resolved, surface sensitive, sub-micron resolution wide field thermal imaging technique, exploiting fast radiative recombination rates of quantum rod photoluminescence to probe temperature transients in semiconductor devices. We demonstrate a time resolution of 20 μs on a single finger AlGaN/GaN HEMT. This technique provides an image of the surface temperature transients regardless of the device design/material system under test. The results were verified with transient thermo-reflectance measurements.**

Index Terms— GaN HEMT, hyperspectral quantum rod thermography, thermal metrology, transient self-heating.

I. Introduction

INCORPORATING thermal considerations into device design is vital for an efficient and reliable device and circuit operation as device life time and operation is highly temperature dependent [1, 2]. Temperature measurements are therefore critical to support device designs and for device lifetime estimations; they are also commonly used as an input parameter for compact electro-thermal modeling [3].

There are numerous steady state thermal characterization techniques for semiconductor devices, the most popular of which are electrical methods such as resistance thermometry [4], optical techniques such as transient thermo-reflectance (TTR) imaging [5, 6, 7], Raman thermography [8], IR thermography [9] and contact methods such as scanning thermal microscopy (SThM) [10]. Steady state thermal measurements are useful for thermal performance benchmarking; yet, the transient temperature during dynamic operation needs to be considered, e.g., the real operating condition of pulsed devices.

Transient temperature measurements, with the sub-micron resolution needed for much of todays' microelectronics, are challenging. Unknown thermo-reflectance coefficients in addition to effects of sub-surface reflections make TTR imaging complex for devices with multiple surface types [11]. Transient Raman thermography enables submicron spatial resolution and nanosecond time resolution but requires serial point by point acquisitions which is time consuming [12].

We have recently demonstrated hyperspectral quantum rod thermal imaging (HQTI), exploiting the temperature dependent emission wavelength of quantum rods, deposited on a device surface and measured using a hyperspectral camera [13]. This has enabled accurate, fast, sub-micron spatial resolution, large area surface temperature mapping [13]. We demonstrated a temperature precision of ~4 ºC with ~700 nm lateral resolution for steady state measurements of a GaN high electron mobility transistor (HEMT) [13]. In this letter, we report on the development of the transient HQTI technique for time-resolved temperature measurements in devices during pulsed operation.

II. Experimental details

HQTI exploits the temperature dependent emission wavelength of QR nanoparticles deposited on top of the device under test (DUT) [13]. Here we consider a 200×10 μm single finger, field plated, passivated (800 nm thick SiO_2/Si_3N_4), normally-OFF AlGaN/GaN HEMT device, formed by a 80 nm thick AlGaN barrier grown on a 0.75 μm thick GaN, which is on a 700 μm thick Si substrate with a 3.7 μm-thick strain relief layer (SRL).

CdSe/CdS core and shell QRs with 560±20 nm peak emission wavelength were drop cast onto the surface of the passivated device using the method described in [13], with a layer thickness of ≤500 nm [13]. These were excited with an above-band gap 450-nm-LED. Photoluminescence (PL) from an ~95 μm × 125 μm area was collected using a Leica 50× 0.5 NA objective lens and imaged using a hyperspectral camera, as illustrated in Fig. 1.

The hyperspectral camera configuration consists of a tuneable liquid crystal filter and a monochrome camera. The transmission of the filter is tuned by applying a control voltage. A comprehensive description of the steady state HQTI method can be found in [13]. Time resolution was achieved by using a boxcar averaging method. The device pulses and the LED pulses were generated by Tabor 8500, 50 MHz and Agilent 8114 A, 15 MHz pulse generators, respectively; the camera

Manuscript submitted on March 13, 2020. This work was partially funded by the Engineering and Physical Sciences Research Council (EPSRC) under Program Grant GaN-DaME (EP/P00945X/1). (Corresponding authors: B. Ö;

M. K. B. Ö, J.W.P and M. K are with the Centre for Device Thermography and Reliability, University of Bristol, Bristol BS8 1TH, U.K. (e-mail: bahar.oner@bristol.ac.uk; Martin.Kuball@bristol.ac.uk).

This article has been accepted for publication in a future issue of this journal, but has not been fully edited. Content may change prior to final publication. Citation information: DOI 10.1109/LED.2020.2989919, IEEE Electron Device Letters

operated in CW mode as shown in Fig. 1. The time delay between the LED pulse and the device pulse was adjusted such that the LED is turned ON at a desired time interval, which determines the duration of the measurement; the time resolution is determined by the LED pulse length. The gate electrode was continuously pulsed with a period of T=200 µs with 50% duty cycle, between off and on state, with the off state being V_{gs}= 5 V, the on state V_{gs}= 0 V, while V_{ds} was kept constant at 11 V (I_{ds}=84 mA; Joule heating of 0.46 W/mm). The optical heating due to the incident LED light can be neglected (<10 mW/mm^2) and is below the GaN bandgap so as not to generate photo current in the DUT.

The change in emission peak wavelength of the QR was fitted empirically by:

$$\Delta\lambda(T_{rise}) = \alpha T_{rise} + \beta T_{rise}^2 \quad (1)$$

where α =0.072±0.004 nm/ºC and β = (3.45 ± 0.42)×10^{-4} nm/ºC^2; the calibration method, which is equipment dependent (device independent) and only one-off, is reported in [13]. T_{rise} is the temperature rise between on and off state of the device.

The total data acquisition time for a single image at a particular wavelength is 7-8 s for our optical configuration, which can vary depending on the signal to noise ratio. Temperature measurements were performed on a six inch wafer mounted on a thermoelectric vacuum chuck set at 25 ºC. All temperature measurements were taken with the device in equilibrium, i.e., waiting until the device had warmed up.

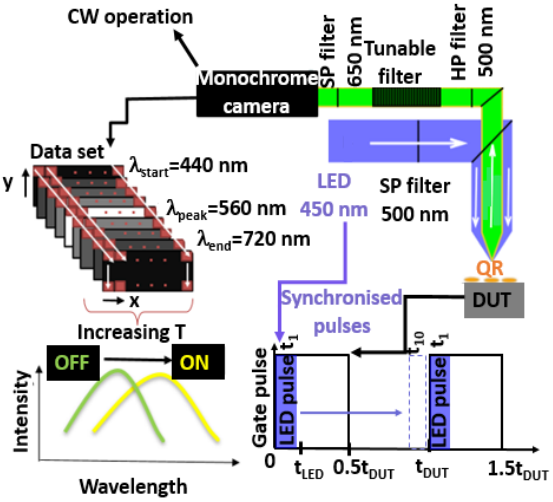

Fig.1. The schematic of the working principle of the transient HQTI set-up.

To validate T-HQTI measurements, we performed transient thermo-reflectance (TTR) measurements on the source connected field plate metal in the middle of the device width with 532 nm CW laser with the same objective lens used for T-HQTI measurements, resulting in ~0.5 µm spatial resolution, which is comparable to that of T-HQTI measurements. As the field plate metal (gold) is opaque under 532 nm, the previously mentioned interference effects in TTR measurements are absent for this point measurement. The TTR set-up is identical to the one described in our previous work [6]. The device operating conditions were identical for T-HQTI and TTR measurements. The schematics of the measurement locations on the device and

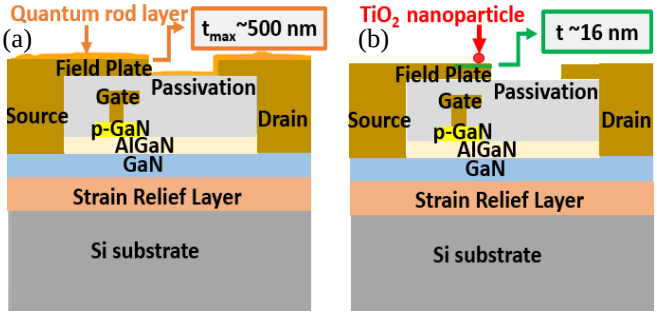

Fig.2. The schematics of the location of the temperature measurements and their corresponding depth resolution on the DUT (not to scale). (a) Location and depth resolution of the T-HQTI measurements. (b) Location and depth resolution of the TTR (green) and TiO_2 assisted (red) transient Raman measurements.

their corresponding depth resolutions are shown in Fig.2. The reflected surface signal originates from the small skin depth of the 532 nm wavelength in the gold (~16 nm [14]), as illustrated in Fig.2b. Temperature rise ($\Delta T=T-T_{ref}$) is related to the reflected signal, following the relation [6]:

$$\frac{R - R_{ref}}{R_{ref}} = C_{th} \cdot (T - T_{ref}) \quad (2)$$

where C_{th} is the material and wavelength dependent thermo-reflectance coefficient, $\Delta R=R-R_{ref}$ is the temperature induced change in the reflectivity with respect to a reference condition.

Calibration of C_{th} is susceptible to large errors, as has been discussed extensively in the literature [6, 15]. Various methodologies have been proposed to extract C_{th} with the minimum error possible, such as using a combination of standard Raman thermography and thermal modelling [6] or using a hot-plate with piezoelectric stage correction to account for thermal expansion [16]. We used an alternative approach for TTR calibration: Transient Raman nano-thermometry, which uses 30-nm-size TiO_2 nanoparticles [17] to measure the surface temperature at precisely the same location as the TTR measurements. We note that even though lateral spatial resolutions of two measurements are different, i.e. 30 nm vs ~0.5 µm, the measured signals represent similar quantities because the temperature gradient on the field plate metal is less than the measurement accuracy (~±5 ºC) there, as shown in our previous work for a device design at the same scale [18].

III. Results and Discussion

Fig. 3 shows the time resolved HQTI surface temperature measurement results along with the optical image of the DUT. The surface transients show the expected trend qualitatively: a rising temperature transient when the device is on and a falling transient when the device is pinched-off, the channel being the hottest region due to its highest resistance. Fig.4 shows the comparison of TTR and T-HQTI measurements performed on sister devices at identical operating conditions.

Both measurements represent the temperature rise of the source field plate metal. Given the error bars, Fig.4 shows that both measurements yield similar results, within the experimental error bar; we note that TTR is a point measurement and T-HQTI is averaged over ~81 µm along the gate width, and small differences may arise from point

This article has been accepted for publication in a future issue of this journal, but has not been fully edited. Content may change prior to final publication. Citation information: DOI 10.1109/LED.2020.2989919, IEEE Electron Device Letters

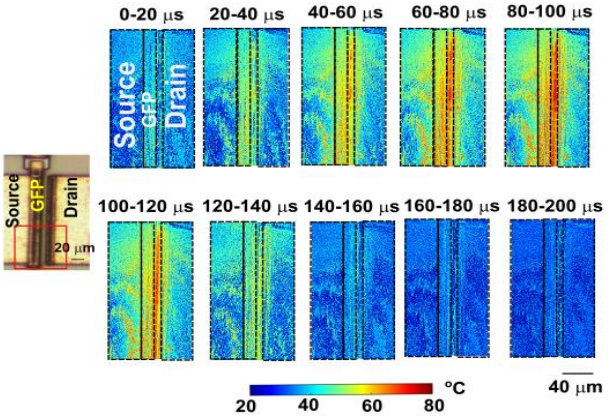

Fig.3. Temperature transients (absolute) of the DUT during the device pulse period, measured with time resolved HQTI along with the optical image of the DUT at the far left. The circled rectangle shows the region where T-HQTI maps corresponds to. 0-100 µs: heating cycle; 100-200 µs: cooling cycle.

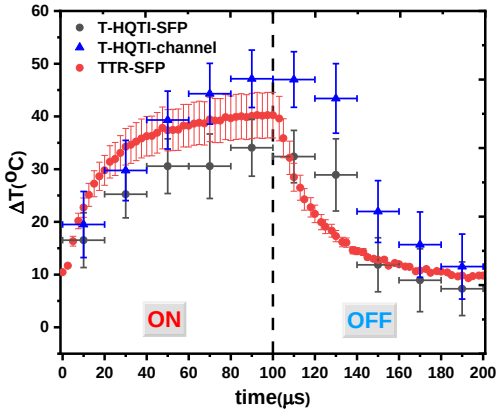

Fig.4. Comparison of TTR and T-HQTI measurements on the source connected field plate (SFP) metal of the GaN HEMT device. ΔT corresponds to temperature rise with respect to the OFF state. Channel temperature was added for comparison.

to point sample variations. Measured surface temperature variations of a similar magnitude are observed in Fig. 3 when the device is off and a uniform temperature is expected, which suggests a systematic offset depending on the location. This artefact may be attributed to the signal-to-noise ratio variations due to QR layer coverage, leading to location dependent variations in the precision. The reasonable agreement between T-HQTI and TTR measurements suggests that 500 nm thick QR coating layer has negligible effect on the heat transport under the considered time scales and thus T-HQTI measurements can be considered as "effective surface" temperature. T-HQTI and TTR. We note that at faster operating regimes, for example, in the GHz range, it is important to consider the time required for the QR layer to reach quasi-equilibrium with the surface of the DUT, though for the MHz range used here this can be neglected.

For the TTR measurements a thermo-reflectance coefficient calibration of C_{th}=4.25×10^{-2}±2.97×10^{-3} was extracted as shown in Fig.5 correlating TiO_2 nanoparticle assisted transient Raman measurements performed at 20 µs time intervals with 20 µs time resolution (optical pulse width), as shown at the inset of Fig.5,

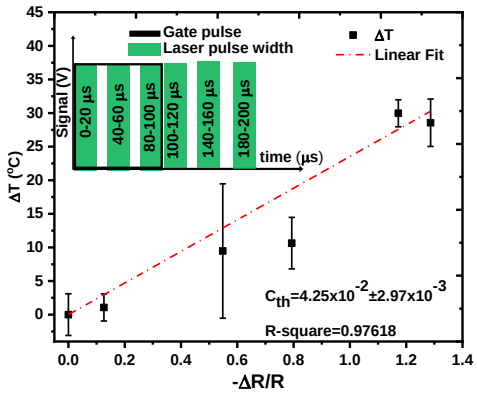

Fig.5. Calibration of TTR signal with the TiO_2 assisted transient Raman measurements. ΔT is with respect to T_{ref} which is the TiO_2 temperature at Δt=190±10 µs. The inset shows the time intervals at which TiO_2 assisted Raman measurements were performed (green laser pulses) and the gate pulse.

with the reflectivity change using (2). C_{th} is typically in the 10^{-2}-10^{-5} ^{o}C^{-1} range, depending on the material, illumination wavelength, optical set-up and surface roughness [19]. In the literature, C_{th} of gold is reported to be in the 10^{-3} [20, 21]-10^{-4} [19, 15] ^{o}C^{-1} range for 530 nm excitation. Our one order of magnitude higher estimation could be due to the highly rough metal surface, which is optically visible, and the optical set-up. This estimation highlights the need for *in situ* calibration for each particular test structure for thermo-reflectance based thermal imaging.

The ultimate time resolution achievable with the T-HQTI measurements is limited by the radiative life-time of the QRs. We demonstrated here 20 µs time resolution (MHz regime) due to the limitations of the rise time of the pulse generator used for the LED pulsing in our test set-up. However, time resolution of this technique can be extended down to 10 ns for the QRs considered here [22] with small modifications in the test set-up. Alternatively, time gated cameras which are currently commercially available down to ps gating, rather than CW operation, can be used, depending on the application.

IV. Conclusion

We demonstrated a hyperspectral and quantum rod based thermal imaging technique for studying pulsed operated devices, illustrated on GaN HEMTs, allowing time resolved sub-micron resolution temperature mapping measurements in the MHz regime. The main advantages are that the technique requires only one-off calibration, and is device independent, and enables full and fast device thermal imaging; it has the potential to be extended for GHz range time resolution surface temperature imaging of semiconductor devices.

Acknowledgment

The authors thank Infineon Technologies for providing the devices used in this work. B.Ö. thanks Infineon Technologies and University of Bristol Alumni Foundation for the PhD sponsorship.

REFERENCES

[1] M. White and J. B. Bernstein, "Microelectronics Reliability: Physics-of-Failure Based Modeling and Lifetime Evaluation," JPL Publication, Pasadena, 2008.

[2] A. Bensoussan, "Microelectronic reliability models for more than moore nanotechnology products," *Facta Universitatis, Series: Electronics and Energetics*, vol. 30, no. 1, pp. 1-26, 2017. DOI: 10.2298/FUEE1701001B

[3] S. Ono, M. Ciappa, S. Hiura and W. Ficht, "Electro-thermal simulation in the time domain of GaN HEMT for RF switch-mode amplifier," *Microelectron. Rel.,* vol. 52, no. 9-10, pp. 2224-2227, 2012. DOI: 10.1016/j.microrel.2012.06.063

[4] G. Pavlidis, D. Kendig, E. R. Heller and S. Graham, "Transient thermal characterization of AlGaN/GaN HEMTs under pulsed biasing," *IEEE Trans. Electron Devices*, vol. 65, no. 5, pp. 1753-1758, 2018. DOI: 10.1109/TED.2018.2818621

[5] G. Tessier, . M. L. Polignano, S. Pavageau, C. Filloy, D. Fournier, F. Cerutti and I. Mica, "Thermoreflectance temperature imaging of integrated circuits: Calibration technique and quantitative comparison with integrated sensors and simulations," *J. of Phys. D: Appl. Phys.,* vol. 39, no. 19, pp. 4159-4166, 2006. DOI: 10.1088/0022-3727/39/19/007

[6] S. Martin-Horcajo, J. W. Pomeroy, B. Lambert, H. Jung, H. Blanck and M. Kuball, "Transient thermoreflectance for gate temperature assessment in pulse operated GaN-based HEMTs," *IEEE Electron Device Lett.,* vol. 37, no. 9, pp. 1197-1200, 2016. DOI: 10.1109/LED.2016.2595400

[7] J. Christofferson and A. Shakouri, "Thermoreflectance based thermal microscope," *Rev. Sci. Instrum.,* vol. 76, p. 024903, 2015. DOI: 10.1063/1.1850632

[8] M. Kuball, J. M. Hayes, M. J. Uren, T. Martin, J. C. Birbeck, R. S. Balmer and B. T. Hughes, "Measurement of temperature in active high-power AlGaN/GaN HFETs using Raman spectroscopy," *IEEE Electron Device Lett.* , vol. 23, pp. 7-9, 2002. DOI: 10.1109/55.974795

[9] D. L. Blackburn, "A review of thermal characterisation of power transistors," in *Proc. 20th IEEE Semicond. Therm. Meas. Managa. Symp.*, San Diego, CA,USA, 1988. DOI: 10.1109/SEMTHE.1988.10589

[10] D. G. Cahill, K. Goodson and A. Majumdar, "Thermometry and thermal transport in micro/nanoscale solid-state devices and structures," *J.Heat Transfer* , vol. 124, pp. 223-241, 2002. DOI: 10.1115/1.1454111

[11] D. Kendig, K. Yazawa and A. Shakouri, "Hyperspectral Thermoreflectance Imaging for Power Devices," in *EEE 33rd SEMI-THERM Symposium*, San Jose, CA, USA, 2017. DOI: 10.1109/SEMI-THERM.2017.7896931

[12] M. Kuball, G. J. Riedel, J. W. Pomeroy, A. Saura, M. J. Uren, T. Martin, K. P. Hilton, J. O. Maclean and D. J. and Wallis, "Time-resolved temperature measurement of AlGaN/GaN electronic devices using micro-Raman spectroscopy," *IEEE Electron Device Lett.,* vol. 28, no. 2, pp. 86-89, 2007. DOI: 10.1109/LED.2006.889215

[13] B. Öner , J. W. Pomeroy and M. Kuball, "Submicron resolution hyperspectral quantum rod thermal imaging of microelectronic devices," *ACS Applied Elect. Mat.*,vol. 2, no.1, pp.93-102 2020, DOI: 10.1021/acsaelm.9b00575.

[14] D. I. Yakubovsky, A. Arsenin, Y. V. Stebunov, D. Y. Fedyanin and V. Volkov, "Optical constants and structural properties of thin gold films," *Opt.Exp.,* vol. 25, no. 21, pp. 25574-25587, 2017. DOI: 10.1364/OE.25.025574

[15] T. Favaloro, J. H. Bahk and A. Shakouri, "Characterization of the temperature dependence of the thermoreflectance coefficient for conductive thin films," *Rev. Sci. Instrum.,* vol. 86, pp. 024903-1-024903-8, 2015. DOI: 10.1063/1.4907354

[16] A. Shakouri, A. Ziabari, D. Kendig, J. H. Bahk, Y. Xuan, P. D. Ye, K. Yazawa and A. Shakouri, "Stable thermoreflectance thermal imaging microscopy with piezoelectric position control," in *Annual IEEE Semiconductor Thermal Measurement and Management Symposium*, San Jose, CA, USA, 2016. DOI:10.1109/SEMI-THERM.2016.7458456

[17] J. Anaya, T. Bai, Y. Wang, C. Li, M. Goorsky, T. L. Bougher, L. Yates, Z. Cheng, S. Graham, K. D. Hobart, T. I. Feygelson, M. J. Tadjer, T. J. Anderson, B. B. Pate and M. Kuball, "Simultaneous determination of the lattice thermal conductivity and grain/grain thermal resistance n pollycrystalline diamond," *Acta Materialia,* vol. 139, pp. 215–225, 2017. DOI: 10.1016/j.actamat.2017.08.007

[18] J. W. Pomeroy, M. J. Uren, B. Lambert and M. Kuball, "Operating channel temperature in GaN HEMTs: DC versus RF accelerated life testing," *Microelectronics Reliability,* vol. 55, pp. 2505–2510, 2015. DOI: 10.1016/j.microrel.2015.09.025

[19] M. Farzaneh, K. Maize, D. Lüerßen, J. A. Summers, P. M. Mayer, P. E. Raad, K. P. Pipe, A. Shakouri, R. J. Ram and J. A. Hudgings, "CCD-based thermoreflectance microscopy: principles and applications," *J. of Phys. D: Appl. Phys.,* vol. 42, no. 14, p. 143001, 2009. DOI: 10.1088/0022-3727/42/14/143001

[20] R. B. Wilson, B. A. Apgar, L. W. Martin and D. G. Cahill, "Thermoreflectance of metal transducers for optical pump-probe studies of thermal properties," *Opt. Exp.,* vol. 20, no. 27, pp.28829-28838, 2012. DOI: 10.1364/OE.20.028829

[21] D. U. Kim, K. S. Park , C. B. Jeong , G. H. Kim and K. S. Chang , "Quantitative temperature measurement of multi-layered semiconductor devices using spectroscopic thermoreflectance microscopy," *Opt. Exp.,* vol. 24, no. 13, pp. 13906-16, 2016. DOI: 10.1364/OE.24.013906

[22] M. Pelton, J. J. Andrews, I. Fedin, D. V. Talapin, H. Leng and S. K. O'Leary, "Nonmonotonic Dependence of Auger Recombination Rate on Shell Thickness for CdSe/CdS Core/Shell Nanoplatelets," *Nano Lett.,* vol. 17, no. 11, pp. 6900–6906, 2017. DOI: 10.1021/acs.nanolett.7b03294